Article

A Novel Microfluidics Droplet-Based Interdigitated Ring-Shaped Electrode Sensor for Lab-on-a-Chip Applications

Salomao Moraes da Silva Junior * , Luiz Eduardo Bento Ribeiro , Fabiano Fruett , Johan Stiens , Jacobus Willibrordus Swart , Stanislav Moshkalev

Posted Date: 3 April 2024

doi: 10.20944/preprints202404.0289.v1

Keywords: Microfluidics devices, Droplet-based Microfluidics, Lab-On-a-Chip sensor, Interdigitated electrodes, Spectroscopic Sensing, Real-time, Microfabrication and Soft Lithography.

Article

A Novel Microfluidics Droplet-Based Interdigitated Ring-Shaped Electrode Sensor for Lab-On-a-Chip Applications

Salomão Moraes da Silva Junior [1,2,3,4,*], Luiz Eduardo Bento Ribeiro [3], Fabiano Fruett [3], Johan Stiens [1], Jacobus Willibrordus Swart [3] and Stanislav Moshkalev [2]

[1] Electronics & Informatics, Vrije Universiteit of Brussel, Brussels 1050, Belgium

[2] Center for Semiconductor Components and Nanotechnologies, State University of Campinas, Campinas 13083-852, Brazil

[3] School of Electrical and Computer Engineering, State University of Campinas, Campinas 13083-852, Brazil

[4] BioSense Institute, University of Novi Sad, Novi Sad 21000, Serbia

* Correspondence: salomaomoraes@yahoo.com.br

Abstract: Droplet-based microfluidics has revolutionized numerous fields such as biomedical research, pharmaceuticals, drug discovery, food engineering, flow chemistry, and cosmetics. This paper presents a comprehensive study focusing on the detection and characterization of droplets with volumes in the nanoliter range. Leveraging the precise control of minute liquid volumes, we introduced a novel spectroscopic On-Chip microsensor equipped with integrated microfluidic channels for droplet generation, characterization, and sensing, simultaneously. The microsensor, designed with Interdigitated-Ring-Shaped Electrodes (IRSE) and seamlessly integrated with microfluidic channels, offers enhanced capacitance and impedance signal amplitudes, reproducibility, and reliability in droplet analysis. We were able to make analyses of droplets length in the range 1.0-6.0 mm, velocity 0.66-2.51 mm/s, droplet volume 1.07nL-113.46nL. Experimental results demonstrated that the microsensor's has a great performance in terms of droplet size, velocity, and length, with a significant signal amplitude of capacitance and impedance, and real-time detection capabilities, thereby highlighting its potential for facilitating microcapsule reactions and enabling on-site real-time detection for chemical and biosensor analyses on-chip.

Keywords: microfluidics devices; droplet-based microfluidics; Lab-On-a-Chip sensor; interdigitated electrodes; spectroscopic sensing; real-time; microfabrication and soft lithography

1. Introduction

Microfluidics has received increasing attention in a broad spectrum of research fields from fluid physics to biomedicine due to its capability to handle very small amounts of reactants with a high degree of precision, reliability, reproducibility and accuracy[1–5]. Microfluidics devices are commonly called Lab-On-a-Chip (LoC), where micro channels can incorporate multiple unit operations[6–8], that to some extent, replace benchtop laboratory equipment, performing different tasks such as mixing [9], separation, heating and detection. Benefits of microfluidics technology are based on small volume of liquid samples [10], that enables faster chemical reactions process [11,12] due to acceleration of the mass and heat transfer in the microscale [13,14] and integrated micro actuators [15–17]. In the last decades, a microfluidics droplet-based approach has been fast evolved [14,18–21], largely employed for biomedical applications[16,22,23], especially leading to studies with cells and antibody development [20,24,25], where microfluidics devices have enabled a creation of new tools and protocols[16,26–28], for example, for single-cell encapsulation, co-encapsulation, cell-sorting, droplet recovery/extraction (de-oiling) and pico-injection [14,22,24]. Precise control and detection of droplet generation and size are indispensable in numerous microfluidic applications [29–

 doi:10.20944/preprints202404.0289.v1

32], particularly in the field of antibody and drug development [7], including manipulation and delivery in these processes, many of which entail the manipulation of cells or beads, inside of microchannels. Integration of sensing and microfluidics channels [33] are needed, for its importance of generating and monitoring microdroplets [8]. Optical detection [9], impedance detection [10], and capacitive detection [11] emerge as the predominant sensing techniques utilized for droplet size control and detection. However, it is important to mention that optical-based droplet detection often demands a considerably intricate setup external to the device, involving the introduction of laser light and the subsequent detection of scattered light using optical elements positioned within a microfluidic channel or chamber, as evidenced by studies [12,13]. Optics-based interrogation dependence of external equipment does not allow the fabrication of portable point-of-care (POC) [18,34]. Electrochemical sensors can be relatively easier to manufacture and, depending on the specific use case, enable compact circuitry for small and portable devices [10,35,36]. Nonetheless, these sensors have critical limitations, even a very small current passing through the fluid at the open electrode can trigger unwanted reactions such as oxidation, reduction, corrosion, degradation leading to inaccurate readings [36,37]. As a result, by affecting sensor longevity and reliability over time, they may not be ideal for long-term monitoring applications. Additionally, it may require more frequent replacement and calibration due to batch-to-batch variation [36]. On the other hand, insulated electrodes enable a label-free [38,39] and contactless detection avoiding the degradation on the electrode surface [35,40], as the fluid solutions, their continuous and dispersive phases, pass over a passivation layer. In this sense, oil droplets in aqueous solution changing the global capacitance and impedance respond proportionally to the volume of liquids. Sensitivity of sensor response is directly proportional to the electrode surface/wetted area [40], as the electrode's geometry gets covered by the droplet composition [35,40]. It is important to note that the fabrication process and performance of planar interdigitated electrodes may vary depending on the specific application and requirements. In order to optimize the fabrication process [37] and enhance the performance of planar interdigitated electrodes, it is crucial to consider the specific application and requirements of the device, as well as the materials and techniques used in the fabrication process [10,35,36].

In this study, we introduced a novel design of electrodes for the microfluidics sensor, called here the Interdigitated-Ring-Shaped-Electrode (IRSE), which is fully integrated into a low-cost droplet-based microfluidics platform. We demonstrated precise control and characterization of micro droplets, providing basic droplets parameters such as size, volume, velocity, and shape. We presented a fully integrated microfluidics system capable of detecting oil/water and water/oil emulsions, enabling the simultaneous acquisition of impedance and capacitance spectroscopic data, synchronized with video recording. The structure of the IRSE was designed to optimize the capacitance/impedance per unit area ratio, resulting in higher sensitivity, reproducibility, and reliability within a delimited wetted sensing region. Through the integration of the IRSE design into the droplet-based microfluidic architecture, we enhanced the capability for precise characterization of microdroplets for Lab-On-a-Chip applications.

2. Experimental

2.1. Microfluidic Channel Fabrication and Sensor Integration

A microfluidic channel was fabricated using soft-lithography technique, reported in our previous works [11,33]. The master-mold for microfluidic channel was fabricated using conventional contact photolithography, see Figure 1. The microchannel design pattern was transferred to a silicon wafer coated with SU-8 100 photoresist. A few microchannel replicas were fabricated, using a monomer material (Sylgard 184) deposited onto master-mold. The monomer material used was Polydimethylsiloxane (PDMS), a layer of PDMS was deposited in the SU-8 mold. PDMS is comprised of two parts, curing agent and prepolymer base, they were stirringly mixed at a 1:10 weight ratio. The mixture was poured onto a replication master and degassed in a desiccator with 5.3–6.7 Pa for 120 minutes, to eliminate all trapped air bubbles in the mixture.

 doi:10.20944/preprints202404.0289.v1

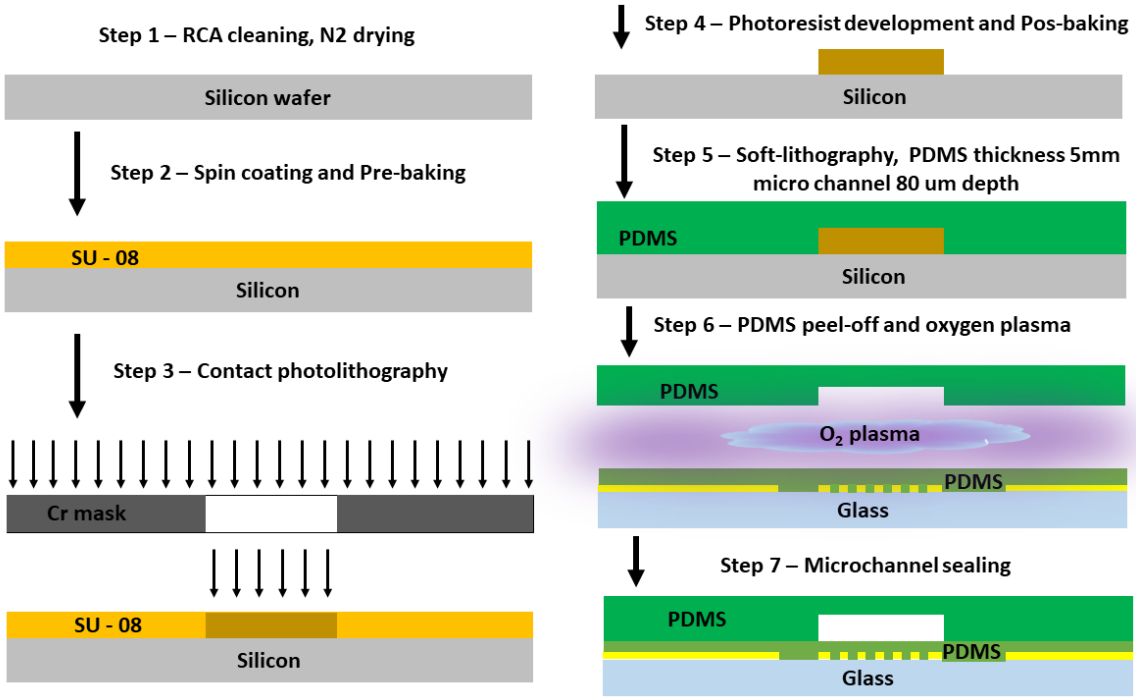

Figure 1. Microchannel fabrication. SU-8 master mold replica, soft-lithography, and microchannel cover.

The master-mold was fully covered with uncured PDMS mixture; the next step was to get the polymer cured. The curing process was carried out for 60 minutes on a hot plate at 100°C, and was followed by cooling down to room temperature, to get the peeling-off of the PDMS layer from the mold. Subsequently, microchannel sealing process was carried out with oxygen plasma, by oxidizing PDMS and microscope slides surfaces through RF O_2 plasma (plasma cleaner, PLAB SE80) for 2 minutes. Finally, the PDMS microchannel layer and the glass substrate containing the IRSE were manually aligned under the microscope, and placed together, to allow the complete bonding process between the two surfaces, for 2 hours, finalizing the device fabrication at room temperature, as shown in Figure 1. The channels dimensions were 200µm width, 80µm height and 1cm length.

More details on the fabrication process is presented in the Supplementary Material.

2.2. Experimental Setup

Once fabricated microfluidics chip, we inspected the chips under the microscope and performed the leakages tests. Leakages tests were done with an experimental setup, as shown in Figure 2. To evaluate the droplet formation process, size, and velocity, we attached a CCD camera to microscope and simultaneously we recorded the videos and signal changes generated on the IRSE sensor in the LabVIEW platform.

 doi:10.20944/preprints202404.0289.v1

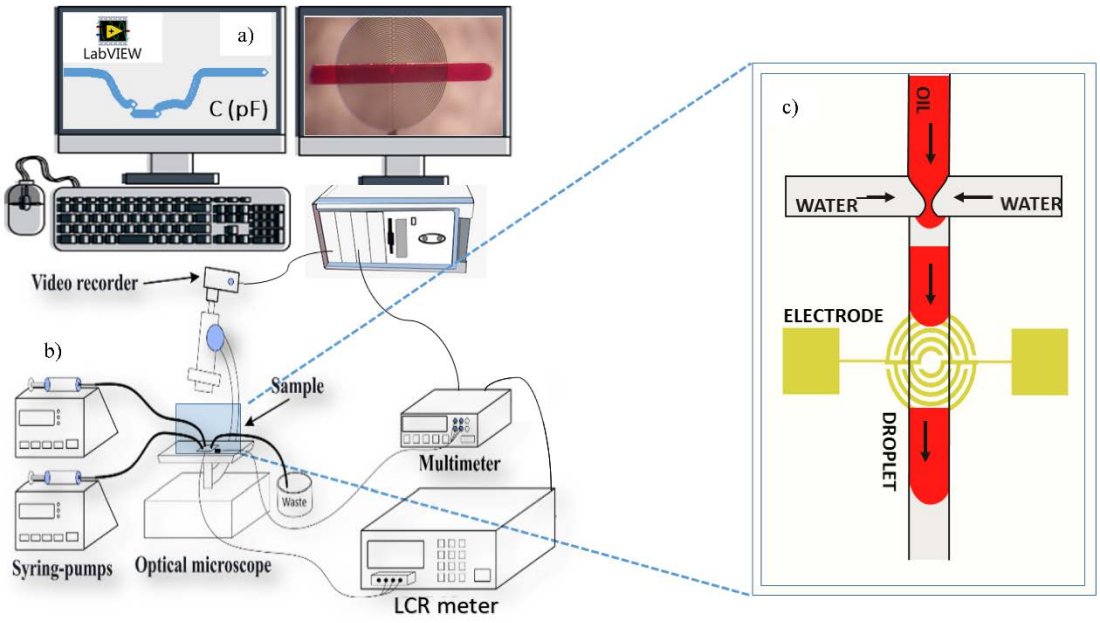

Figure 2. Microfluidics experimental setup used to acquire the capacitive/impedance response. a) LabView user interface and image acquisition. b) Platform with syringe pumps, LCR meter, multimeter and microscope. c) Microfluidics droplet generator with integrated IRSE sensor.

In parallel, we had the LCR meter (Hewlett-Packard, 4284A) connected to IRSE to monitor in real-time the signal changes in terms of capacitance and impedance over the IRSE sensor. The full setup is connected to a computer with software developed in *LabView*®, that makes the data acquisition and displays it. The results and analyses were performed in the post-processed images and videos synchronized with data signal recorded from the sensor over time. Since the fluid permittivity varies with the temperature, the device temperature was monitored to ensure it was kept near to room temperature. We used a benchtop Multimeter (Agilent, 34401A) connected to a thermocouple (PT100) used as a reference temperature sensor placed in contact with the microfluidic chips, as shown in Figure 2.

3. Results and Discussion

Mechanism of Droplet Formation and Detection

Multiphase micro flows are characterized by the ratio of viscous to surface forces, the capillary number (***Ca***) and Webber number (***We***) by the ratio of fluid viscosities, as described in the Equations (1) and (2) [12,41]:

$$Ca = \frac{\mu U_d}{\sigma}\frac{\mu}{\mu_d} \quad (1)$$

And,

$$We = \frac{\rho U_d^2 d_h}{\sigma} \quad (2)$$

where **μ** and **μ**$_d$ are the fluid viscosities of the continuous and the dispersed phases, respectively.

U_d is the velocity, **σ** is the density, ρ is the density and d_h is the hydraulic diameter of the channel.

The ***Ca*** number represents the balance between viscous forces and surface tension forces, while the ***We*** number indicates the relative importance of inertial forces compared to surface tension forces. The interaction between the Capillary and Weber numbers significantly influences the process of droplet formation in microfluidic systems, as shown in Figure 3. At lower ***Ca*** values, where viscous forces are dominant over surface tension forces, droplets formation occurs more slowly and have a

 doi:10.20944/preprints202404.0289.v1

tendency to be more spherical in terms of shape, due to the prevalence of surface tension effects [41]. As ***Ca*** increases, the influence of surface tension decreases, resulting in faster droplet formation and non-spherical shapes as inertial forces become more significant. Similarly, the Weber number has a big impact on droplet formation dynamics.

At low ***We*** values, where surface tension dominates over inertial forces, small spherical droplets can be formed primarily due to surface tension effects. However, at higher ***We*** numbers, inertial force becomes greater leading to quicker droplet generation along with potential for satellite or irregular shaped droplets formations. To determine the type of regime flow, Reynolds number is important, it can be calculated by the ratio of ***We*** and ***Ca***, as follows, ***Re*** = ***We***/***Ca***. Our droplet formation regime flow was defined by a fixed volumetric flow for the dispersive phase (in our case HFE 7500 oil from 3M), of 8, 21 and 34 µL/hour and for the continuous phase (DI water) of 1µL/hour, so Reynolds number can be extracted.

The droplets formation occurs in a very laminar flow regime with ***Re*** ranging from 0.0452 to 0.1357, as shown in Figure 4. Understanding these dynamics is crucial for optimizing processes related to microdroplet generation, stability, controlling, size and shape-wise across droplet-based microfluidics applications platforms.

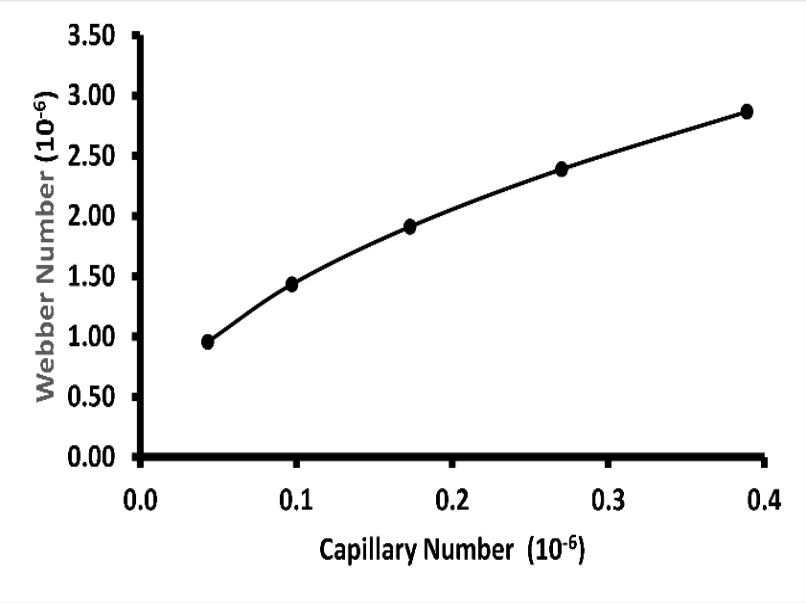

Figure 3. Regime flow relation of Webber and Capillary number in droplet formation dependency.

The IRSE sensor was combined with a double T-junction microchannel to assess the droplet formation, size, and velocity, as shown in . The spontaneous generation of droplets was managed using two syringe pumps (NE100, New Era, US). As previously mentioned, the continuous phase consisted of ultra-pure DI water with a high resistance value (18.2 MΩ.cm), while the dispersed phase comprised fluorinated oil HFE7500. To improve visibility of droplet formation, the dispersed phase was colored red to enhance contrast and enable data synchronization between the camera and sensor.

Preprints.org (www.preprints.org) | NOT PEER-REVIEWED | Posted: 3 April 2024 doi:10.20944/preprints202404.0289.v1

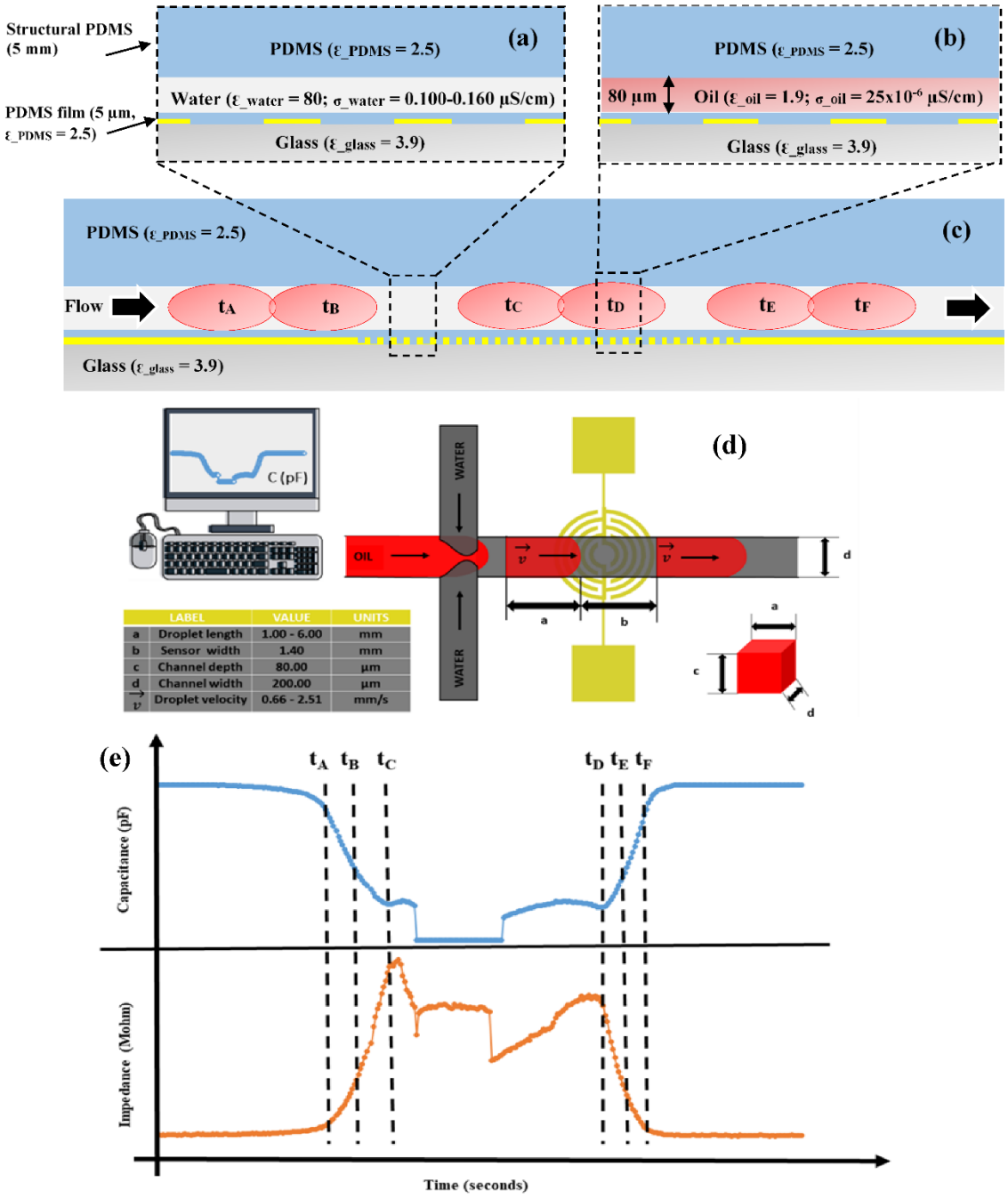

Figure 4. Cross-section of IRSE sensor structure and droplets response. (a) Microfluidics channel filled with the continuous phase, (b) filled with the dispersive phase. (microchannels dimension, dielectric constant of materials and conductivities of liquids are shown). (c) Flow direction and droplets response with droplets movement over time. (d) Droplet generation design in a double-junction channel, spontaneous droplets formation response. (e) Real-time droplet response in capacitance and impedance.

As can be observed in Figure 5, the impedance signal generated by the droplets on the sensor has a peak in 10.60 MΩ, and baseline around 4.60 MΩ leading to a very high signal amplitude of 6 MΩ. On the other hand, in terms of capacitance, the peak was at 2.650×10^{-2} pF and baseline around 2.615×10^{-2} pF leading to a signal amplitude of 35 $\times 10^{-2}$pF, with sensitivity being 12 times higher than described by Ernst et al [38].

 doi:10.20944/preprints202404.0289.v1

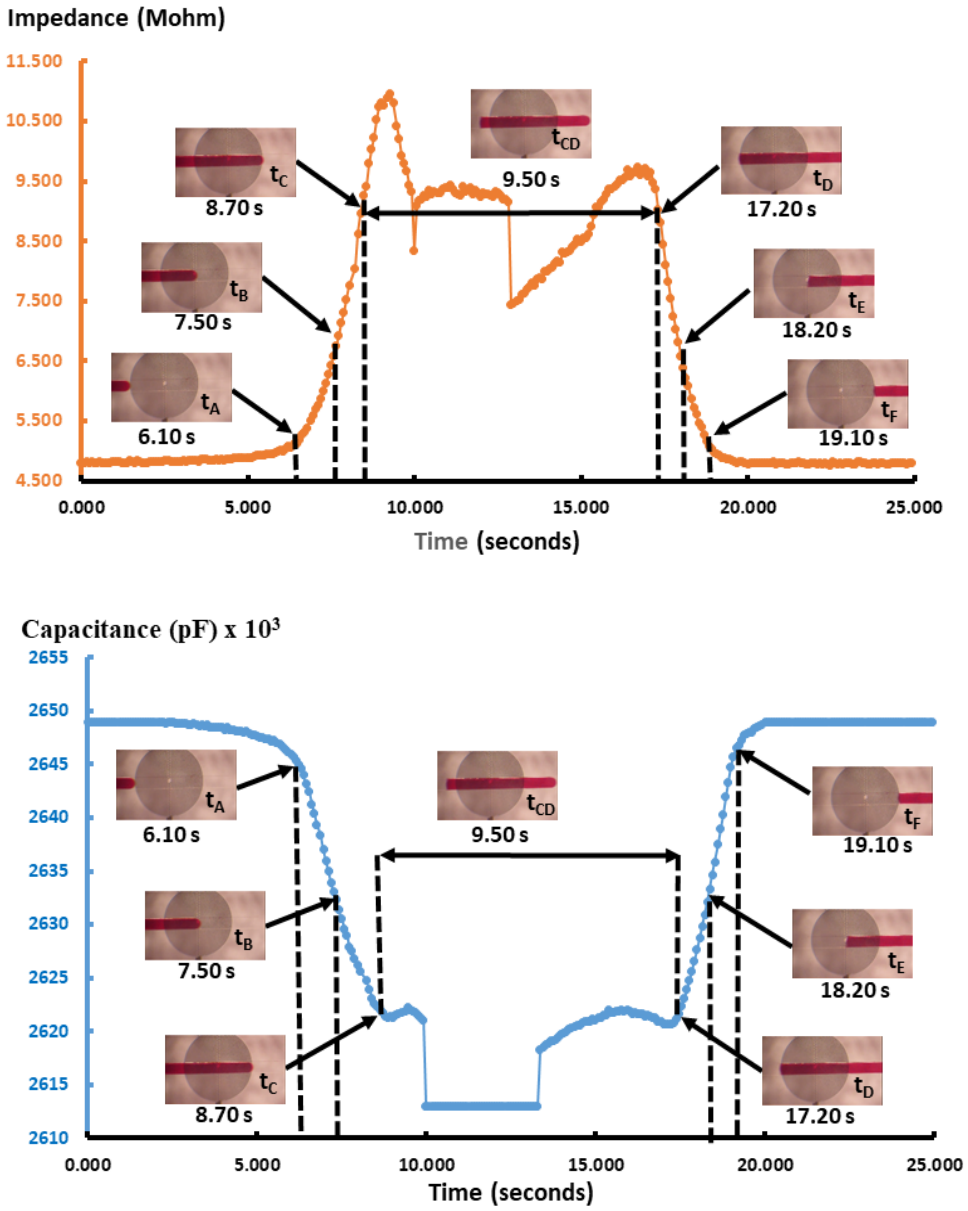

Figure 5. Cross-section of IRSE sensor structure and droplets response. (a) Microfluidics channel filled with continuous phase, (b) filled with dispersive phase, microchannels dimension, dielectric constant of materials and liquids conductivity. (c) Flow direction and droplets response with droplets movement over time. (d) Real-time droplet response, IRSE sensing window, amplitude signals changes versus time (d) capacitive) and (e) impedance, from the show results, it can be determining droplets content, size, and velocity.

Droplet size-wise and shape-wise were determined by a unique pair of volumetric flow rates set on the syringe-pumps. There are three main droplet formation regimes: (i) a dripping regime, which produces small spherical droplets; (ii) a regime of interest with medium-size droplet formation; (iii) a squeezing regime, which produces long plug-like droplets. We used the squeezing regime to evaluate the sensor response, due to limitation in real-time response of the electrode sensor, and wetted area demanded, to avoid false reading of the droplet length that must be equal or bigger to electrode length. On Figure 6 (a) and (b), we delimited the regime flow into three data points, generating as a result three populations of droplet size: small, medium, and large.

 doi:10.20944/preprints202404.0289.v1

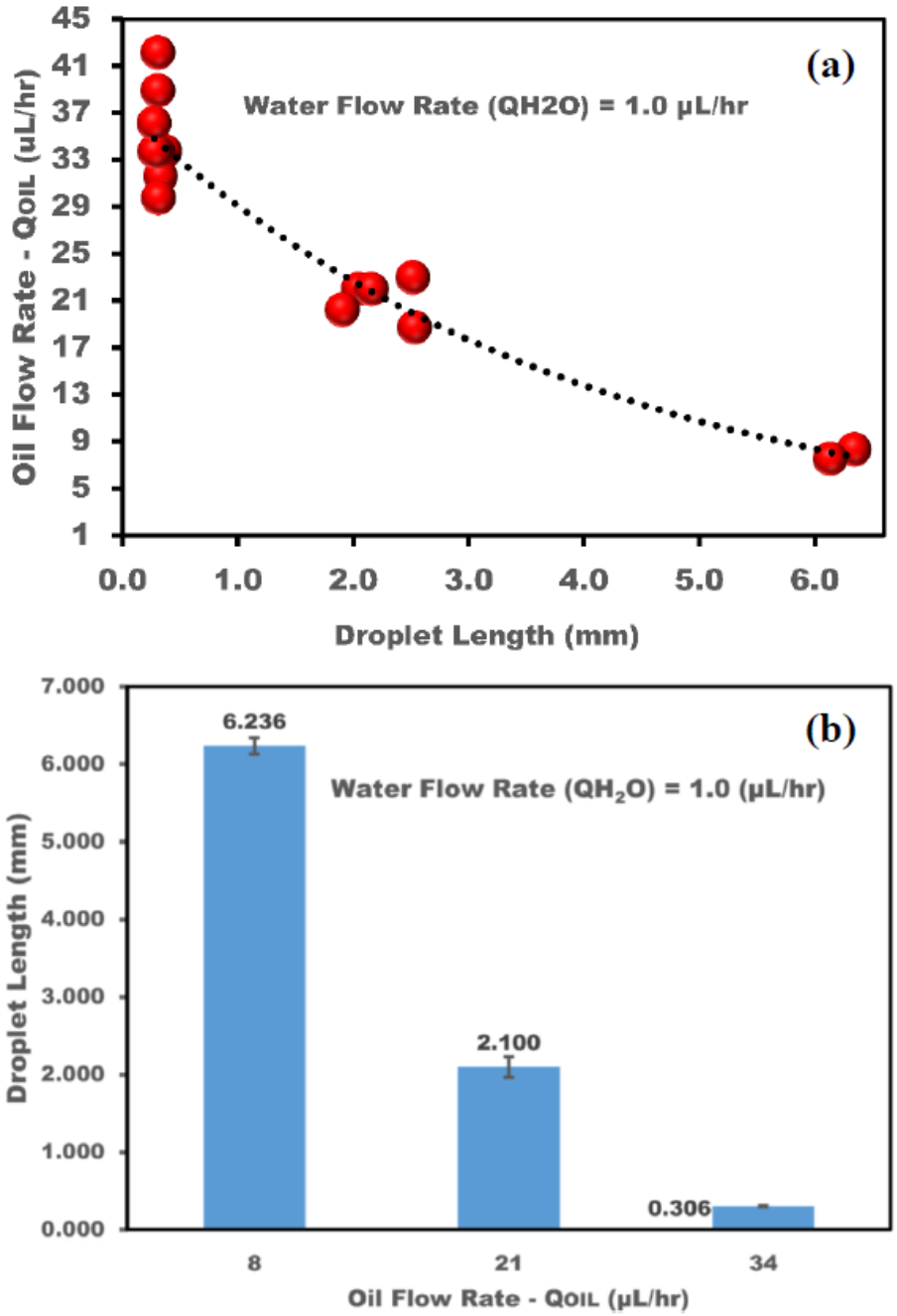

Figure 6. Microchannel droplet formation. (a) Three data points observed droplet size dependency with flow rate. (b) Droplet size distribution and size variation.

In fact, the small group of droplets are not detectable, because the sensor averages the signal and there is no clear response. The impedance and capacitance change dynamically, in accordance with the droplet passage over the IRSE sensor. To relate the output signal to the flow rate parameters, images of droplet formation were captured with a camera coupled to a microscope, and validation of sensor readout with images and video acquired from droplets generation. These enabled measurements of droplet size, length, and volume, validating the sensor readout through videos technique extraction. The Figure 5 presented the data extracted directly from videos synchronized with IRSE sensor response simultaneously.

Employing the methodology of extracting the timestamp from images and videos acquired, and then we multiplied by sensor length. With this approach we were able to estimate the droplet, velocity, length, and volume. The Figure 7 has shown the droplet volume dependency with volumetric flow rate. Note that it is possible to reduce the droplet size to less than the distance

 doi:10.20944/preprints202404.0289.v1

occupied by the sensor increasing the flow of aqueous colorant relative to the oil flow. In this case, the impedance does not reach the peak value, it gets in the middle of the amplitude. Further, if two or more droplets enter the sensor field, the measured value is relative to the average impedance over the IRSE. Each droplet of aqueous colorant represents an increase in IRSE impedance because oil has higher resistance than water, and higher dielectric constant, leading to higher capacitance.

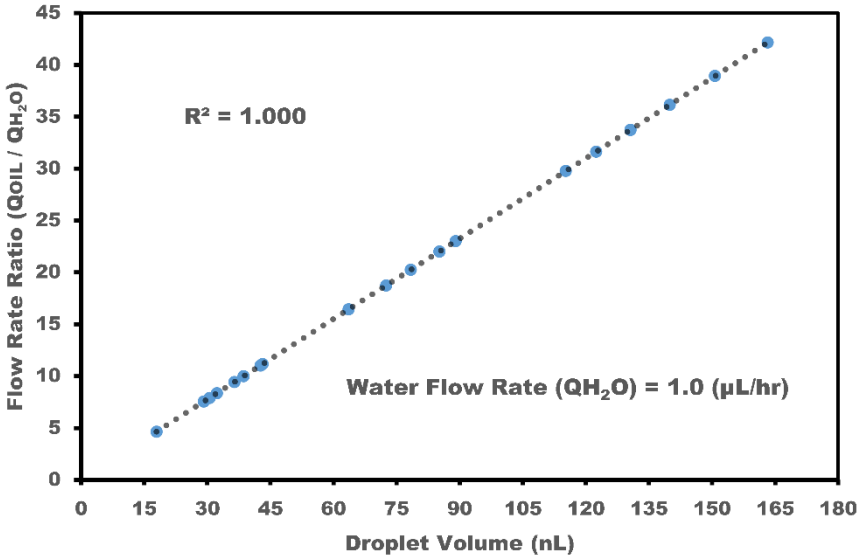

Figure 7. Droplet volume dependency on the volumetric flow rate.

The pulse length when capacitance is over 2.650 x10^{-2} pF determines the time that the droplet was over the IRSE sensor working in a capacitor mode. On the other hand, while the base value is kept when capacitance is about 2.610 x 10^{-2} pF, this determines the period in which the continuous phase fluid is over IRSE. Taking in account the flow rate and the microchannel cross section, the droplet absolute velocity, it can be calculated by the droplet-traveled distance in the microchannel volume that can be taken from is the cross-sectional area of the microchannel and droplet length. We observed that the flow rate imposed a proportional change in velocity and volume of the droplets, as shown in Figure 7. In addition, it relates to the variables of interest such as signal changes, pulse length when impedance is over 10.50 MΩ determines the time that the droplet was over the IRSE sensor working in impedance mode, in other hand while the base value is kept when capacitance is about 4.50MΩ, determines the period in which the continuous phase fluid is over IRSE. Finally, we have presented a fully integrated microfluidics droplet-based system, applied for generation and detection of nano volume range droplets with both impedance and capacitance responses.

It is essential to have additional components in lab-on-a-chip applications due to their complex design and versatility, combining microelectrode sensors and microchannels. These sensors, fabricated in cleanroom environment using precise microfabrication techniques, comprise closely positioned concentric ring-shaped electrodes that allow for efficient handling and detection of analytes, particularly charged species such as ions or biomolecules, in addition, to it providing and sterile cheap suitable for biomedical applications. Due to a very small size and compatibility with microfabrication methods, make it possible to integrate it into microfluidic devices for accurate on-chip detection and analysis of analytes, in this case, we have demonstrated for droplets formation and detection simultaneously. The precise control provided by microfabrication techniques ensures creation of strong and confined electric fields in a small area between the concentric rings 10 µm gap, thus improving sensitivity and enabling dynamic manipulation of analytes within the microfluidic environment. As a result, IRSE sensors are likely to play a crucial role in advancing lab-on-a-chip technology by offering high sensitivity and specificity for various applications, from biomedical diagnostics to environmental monitoring, highlighting their significance in analytical sciences.

 doi:10.20944/preprints202404.0289.v1

4. Conclusion

In this study, we presented the results of development of a novel IRSE (Interdigitated-Ring-Shaped Electrodes) microfluidic device capable of generating and simultaneously characterizing microdroplets with nanoliter volumes. By integrating electrical (capacitive and impedance) and optical (droplet shape and size) characterizations, the system allows to have precise and fully controllable and reproducible generation of droplets. Integration of various on-line characterization technique along with enhanced sensitivity of electrical measurements due to a special design of electrodes is a distinctive feature of the present design, resulting in greatly enhanced functionality of the device.

We employed a Double T-junction shaped microchannel within a multiphase microfluidic system to generate droplets of oil-in-water (o/w). The dispersive phase consisted of oil mixed with a red dye colorant, while the DI water was used as a continuous phase. The real-time synchronization of the sensor data with video recordings facilitated analyses, and validation of all acquired data. Our findings consistently revealed impedance and capacitance variations corresponding to biphasic fluid flowing over the sensor, with signal changes in terms of capacitance $35x10^{-2}$pF and impedance 6.0 MΩ. We were able to make analyses of droplets length in the range 1.0-6.0 mm, velocity 0.66-2.51 mm/s, droplet volume 1.07nL-113.46nL.

The utilization of integrated real-time capacitance and impedance measurements holds significant promise in microfluidic devices, particularly for precise control of valves and pumps to achieve desired droplet sizes in biphasic mixtures. This methodology has a great potential for numerous practical applications, including drug delivery and food encapsulation. Moreover, in the dripping regime, the IRSE sensor allows for estimation of droplet velocity and volume, enhancing its utility in microfluidic systems. The integration of real-time capacitance and impedance measurements into microfluidic platforms offers enhanced control over droplet formation and flow rates, with implications extending across, flow-chemistry, biopharmaceuticals, diagnostics, and chemical synthesis. Furthermore, the IRSE sensor enables real-time monitoring and analysis of droplet dynamics, providing invaluable insights into droplet behavior within microfluidic contexts.

Author Contributions: Conceptualization, S.M.S.J., L.E.B.R. and S.M.; methodology, S.M.S.J. and S.M.; validation, S.M.S.J. and L.E.B.R.; formal analysis, S.M.S.J.; investigation, S.M.S.J., L.E.B.R., J.S. and resources, F.F., J.W.S.; data curation, I.V.M.; writing—original draft preparation, S.M.S.J., L.E.B.R.; writing—review and editing, S.M.S.J. and S.M.; visualization, S.M.S.J.; supervision, F.F., J.S., J.W.S. and S.M.; project administration, S.M.; funding acquisition, J.W.S. and S.M. All authors have read and agreed to the published version of the manuscript.

Funding: The authors thank the University of Campinas (Unicamp): FEEC, the Center for Semiconductor Components and Nanotechnologies (CCSNano), the Multi-User Laboratory of IFGW (LAMULT), the Research Laboratory (LPD) and the Brazilian Synchrotron Laboratory (LNLS) for technical assistance. Financial support for this project was provided by the National Council for Scientific and Technological Development (CNPq) INCT NAMITEC project No. 406193/2022-3, and the scholarship grant from the Amazon Research Foundation (FAPEAM). BeMundus is supported from Erasmus Mundus Program (EU), the Project Horizon 2020. The authors also acknowledge Vrije Universiteit Brussel (VUB) and the LAMI-ETRO team, and for the funding through the SRP-project M3D2 and the IOF-ETRO project. This work was supported by the ANTARES project, which received funding from the European Union's Horizon 2020 research and innovation program under Grant agreement ID: 739570.

Acknowledgments: The authors thank the University of Campinas (Unicamp): FEEC, the Center for Semiconductor Components and Nanotechnologies (CCSNano), the Multi-User Laboratory of IFGW (LAMULT), the Research Laboratory (LPD) and the Brazilian Synchrotron Laboratory (LNLS) for technical assistance. Financial support for this project was provided by the National Council for Scientific and Technological Development (CNPq) INCT NAMITEC project No. 406193/2022-3, and the scholarship grant from the Amazon Research Foundation (FAPEAM). BeMundus is supported from Erasmus Mundus Program (EU), the Project Horizon 2020. The authors also acknowledge Vrije Universiteit Brussel (VUB) and the LAMI-ETRO team, and for the funding through the SRP-project M3D2 and the IOF-ETRO project. This work was supported by the ANTARES project, which received funding from the European Union's Horizon 2020 research and innovation program under Grant agreement ID: 739570.

Conflicts of Interest: The authors declare no conflict of interest.

References

1. Shembekar, N.; Hu, H.; Eustace, D.; Merten, C.A. Single-Cell Droplet Microfluidic Screening for Antibodies Specifically Binding to Target Cells. *Cell Rep.* **2018**, *22*, 2206–2215, doi:10.1016/j.celrep.2018.01.071.
2. Ding, Y.; Howes, P.D.; deMello, A.J. Recent Advances in Droplet Microfluidics. *Anal. Chem.* **2020**, *92*, 132–149, doi:10.1021/acs.analchem.9b05047.
3. Shang, L.; Cheng, Y.; Zhao, Y. Emerging Droplet Microfluidics. *Chem. Rev.* **2017**, *117*, 7964–8040, doi:10.1021/acs.chemrev.6b00848.
4. Huebner, A.; Sharma, S.; Srisa-Art, M.; Hollfelder, F.; Edel, J.B.; deMello, A.J. Microdroplets: A Sea of Applications? *Lab. Chip* **2008**, *8*, 1244, doi:10.1039/b806405a.
5. Teh, S.-Y.; Lin, R.; Hung, L.-H.; Lee, A.P. Droplet Microfluidics. *Lab. Chip* **2008**, *8*, 198, doi:10.1039/b715524g.
6. Atencia, J.; Beebe, D.J. Controlled Microfluidic Interfaces. *Nature* **2005**, *437*, 648–655, doi:10.1038/nature04163.
7. Baroud, C.N.; Gallaire, F.; Dangla, R. Dynamics of Microfluidic Droplets. *Lab. Chip* **2010**, *10*, 2032, doi:10.1039/c001191f.
8. Felton, H.; Hughes, R.; Diaz-Gaxiola, A. Negligible-Cost Microfluidic Device Fabrication Using 3D-Printed Interconnecting Channel Scaffolds. *PLOS ONE* **2021**, *16*, e0245206, doi:10.1371/journal.pone.0245206.
9. Zhang, J.; Xu, W.; Xu, F.; Lu, W.; Hu, L.; Zhou, J.; Zhang, C.; Jiang, Z. Microfluidic Droplet Formation in Co-Flow Devices Fabricated by Micro 3D Printing. *J. Food Eng.* **2021**, *290*, 110212, doi:10.1016/j.jfoodeng.2020.110212.
10. Moiseeva, E.V.; Fletcher, A.A.; Harnett, C.K. Thin-Film Electrode Based Droplet Detection for Microfluidic Systems. *Sens. Actuators B Chem.* **2011**, *155*, 408–414, doi:10.1016/j.snb.2010.11.028.
11. Moraes Da Silva Junior, S.; Stiens, J.; Moshkalev, S.; Willibrordus Swart, J.; Lacerda De Orio, R.; Matvejev, V.; Zhang, Y.; Vandermeiren, W.; De Tandt, C. Microfluidic Devices on Glass for Liquid Mixtures Concentration with Coupled Thz Sensor. *J. Integr. Circuits Syst.* **2018**, *13*, 1–5, doi:10.29292/jics.v13i2.10.
12. Chen, C.; Zhao, Y.; Wang, J.; Zhu, P.; Tian, Y.; Xu, M.; Wang, L.; Huang, X. Passive Mixing inside Microdroplets. *Micromachines* **2018**, *9*, 160, doi:10.3390/mi9040160.
13. Whitesides, G.M. The Origins and the Future of Microfluidics. *Nature* **2006**, *442*, 368–373, doi:10.1038/nature05058.
14. Nan, L.; Zhang, H.; Weitz, D.A.; Shum, H.C. Development and Future of Droplet Microfluidics. *Lab. Chip* **2024**, 10.1039.D3LC00729D, doi:10.1039/D3LC00729D.
15. Zhang, Z.; Kan, J.; Cheng, G.; Wang, H.; Jiang, Y. A Piezoelectric Micropump with an Integrated Sensor Based on Space-Division Multiplexing. *Sens. Actuators Phys.* **2013**, *203*, 29–36, doi:10.1016/j.sna.2013.08.027.
16. Liu, G.; Shen, C.; Yang, Z.; Cai, X.; Zhang, H. A Disposable Piezoelectric Micropump with High Performance for Closed-Loop Insulin Therapy System. *Sens. Actuators Phys.* **2010**, *163*, 291–296, doi:10.1016/j.sna.2010.06.030.
17. Li, L.; Ismagilov, R.F. Protein Crystallization Using Microfluidic Technologies Based on Valves, Droplets, and SlipChip. *Annu. Rev. Biophys.* **2010**, *39*, 139–158, doi:10.1146/annurev.biophys.050708.133630.
18. Belykh, S.S.; Yerin, C.V. Influence of the Microdroplets Sizes of Magnetic Emulsions on the Magneto-Optical Effect. *Phys. Met. Metallogr.* **2024**, doi:10.1134/S0031918X23601415.
19. Utharala, R.; Grab, A.; Vafaizadeh, V.; Peschke, N.; Ballinger, M.; Turei, D.; Tuechler, N.; Ma, W.; Ivanova, O.; Ortiz, A.G.; et al. A Microfluidic Braille Valve Platform for On-Demand Production, Combinatorial Screening and Sorting of Chemically Distinct Droplets. *Nat. Protoc.* **2022**, *17*, 2920–2965, doi:10.1038/s41596-022-00740-4.
20. Xu, Z.; Wang, Y.; Sheng, K.; Rosenthal, R.; Liu, N.; Hua, X.; Zhang, T.; Chen, J.; Song, M.; Lv, Y.; et al. Droplet-Based High-Throughput Single Microbe RNA Sequencing by smRandom-Seq. *Nat. Commun.* **2023**, *14*, 5130, doi:10.1038/s41467-023-40137-9.
21. Cerdeira, A.T.S.; Campos, J.B.L.M.; Miranda, J.M.; Araújo, J.D.P. Review on Microbubbles and Microdroplets Flowing through Microfluidic Geometrical Elements. *Micromachines* **2020**, *11*, 201, doi:10.3390/mi11020201.
22. Sonnen, K.F.; Merten, C.A. Microfluidics as an Emerging Precision Tool in Developmental Biology. *Dev. Cell* **2019**, *48*, 293–311, doi:10.1016/j.devcel.2019.01.015.
23. Niu, X.; Zhang, M.; Peng, S.; Wen, W.; Sheng, P. Real-Time Detection, Control, and Sorting of Microfluidic Droplets. *Biomicrofluidics* **2007**, *1*, 044101, doi:10.1063/1.2795392.
24. Guo, M.T.; Rotem, A.; Heyman, J.A.; Weitz, D.A. Droplet Microfluidics for High-Throughput Biological Assays. *Lab. Chip* **2012**, *12*, 2146, doi:10.1039/c2lc21147e.
25. Xiao, Y.; Huang, Q.; Collins, J.W.; Brouchon, J.; Nelson, J.A.; Niziolek, Z.; O'Neil, A.; Ye, F.; Weitz, D.A.; Heyman, J.A. The Rapid Generation of Cell-Laden, FACS-Compatible Collagen Gels. *Organoids* **2023**, *2*, 204–217, doi:10.3390/organoids2040016.
26. Chia, B.T.; Liao, H.-H.; Yang, Y.-J. A Novel Thermo-Pneumatic Peristaltic Micropump with Low Temperature Elevation on Working Fluid. *Sens. Actuators Phys.* **2011**, *165*, 86–93, doi:10.1016/j.sna.2010.02.018.

27. Scott, R.; Sethu, P.; Harnett, C.K. Three-Dimensional Hydrodynamic Focusing in a Microfluidic Coulter Counter. *Rev. Sci. Instrum.* **2008**, *79*, 046104, doi:10.1063/1.2900010.
28. Uhlen, M.; Quake, S.R. Sequential Sequencing by Synthesis and the Next-Generation Sequencing Revolution. *Trends Biotechnol.* **2023**, *41*, 1565–1572, doi:10.1016/j.tibtech.2023.06.007.
29. Vladisavljević, G.T.; Khalid, N.; Neves, M.A.; Kuroiwa, T.; Nakajima, M.; Uemura, K.; Ichikawa, S.; Kobayashi, I. Industrial Lab-on-a-Chip: Design, Applications and Scale-up for Drug Discovery and Delivery. *Adv. Drug Deliv. Rev.* **2013**, *65*, 1626–1663, doi:10.1016/j.addr.2013.07.017.
30. Nightingale, A.M.; Evans, G.W.H.; Xu, P.; Kim, B.J.; Hassan, S.; Niu, X. Phased Peristaltic Micropumping for Continuous Sampling and Hardcoded Droplet Generation. *Lab. Chip* **2017**, *17*, 1149–1157, doi:10.1039/C6LC01479H.
31. Nightingale, A.M.; Hassan, S.; Evans, G.W.H.; Coleman, S.M.; Niu, X. Nitrate Measurement in Droplet Flow: Gas-Mediated Crosstalk and Correction. *Lab. Chip* **2018**, *18*, 1903–1913, doi:10.1039/C8LC00092A.
32. Nightingale, A.M.; Hassan, S.; Makris, K.; Bhuiyan, W.T.; Harvey, T.J.; Niu, X. Easily Fabricated Monolithic Fluoropolymer Chips for Sensitive Long-Term Absorbance Measurement in Droplet Microfluidics. *RSC Adv.* **2020**, *10*, 30975–30981, doi:10.1039/D0RA05330A.
33. Da Silva Junior, S.M.; Stiens, J.; Moshkalev, S.; Swart, J.W.; Matvejev, V.; Zhang, Y.; De Tandt, C. Subterahertz Sensor in Microfluidic Devices for On-Line Determination and Control of Ethanol Concentration. *J. Vac. Sci. Technol. B Nanotechnol. Microelectron. Mater. Process. Meas. Phenom.* **2017**, *35*, 06GA02, doi:10.1116/1.4991891.
34. Nguyen, N.-T.; Lassemono, S.; Chollet, F.A. Optical Detection for Droplet Size Control in Microfluidic Droplet-Based Analysis Systems. *Sens. Actuators B Chem.* **2006**, *117*, 431–436, doi:10.1016/j.snb.2005.12.010.
35. Ribeiro, L.E.B.; de ALCÂNTARA, G.P.; Andrade, C.M.G.; Fruett, F. Analysis of the Planar Electrode Morphology Applied to Zeolite Based Chemical Sensors. **2015**, *193*.
36. Regiart, M.; Gimenez, A.M.; Lopes, A.T.; Carreño, M.N.P.; Bertotti, M. Ultrasensitive Microfluidic Electrochemical Immunosensor Based on Electrodeposited Nanoporous Gold for SOX-2 Determination. *Anal. Chim. Acta* **2020**, *1127*, 122–130, doi:10.1016/j.aca.2020.06.037.
37. Lee, G.; Lee, J.; Kim, J.; Choi, H.S.; Kim, J.; Lee, S.; Lee, H. Single Microfluidic Electrochemical Sensor System for Simultaneous Multi-Pulmonary Hypertension Biomarker Analyses. *Sci. Rep.* **2017**, *7*, 7545, doi:10.1038/s41598-017-06144-9.
38. Ernst, A.; Streule, W.; Schmitt, N.; Zengerle, R.; Koltay, P. A Capacitive Sensor for Non-Contact Nanoliter Droplet Detection. *Sens. Actuators Phys.* **2009**, *153*, 57–63, doi:10.1016/j.sna.2009.04.023.
39. Kalantarifard, A.; Saateh, A.; Elbuken, C. Label-Free Sensing in Microdroplet-Based Microfluidic Systems. *Chemosensors* **2018**, *6*, 23, doi:10.3390/chemosensors6020023.
40. Bento Ribeiro, L.E.; Piazzetta, M.H.; Gobbi, A.L.; Costa, J.S.; Fracassi Da Silva, J.A.; Fruett, F. Fabrication and Characterization of an Impedance Micro-Bridge for Lab-on-a-Chip. *ECS Trans.* **2010**, *31*, 155–163, doi:10.1149/1.3474154.
41. *Micro Process Engineering: A Comprehensive Handbook*; Wiley-VCH: Weinheim, 2009; ISBN 978-3-527-31550-5.